

LBNL-47144

December, 2000

## Nonlinear QED Effects in Heavy Ion Collisions

Spencer R. Klein

*Nuclear Science Division, Lawrence Berkeley National Laboratory**Berkeley, CA, 94720, USA**E-mail: SRKLEIN@LBL.GOV*

Peripheral collisions of relativistic heavy ions uniquely probe many aspects of QED. Examples include  $e^+e^-$  pair production and nuclear excitation in strong fields. After discussing these reactions, I will draw parallels between  $\gamma \rightarrow e^+e^-$  and  $\gamma \rightarrow q\bar{q}$  and consider partly hadronic reactions. The scattered  $q\bar{q}$  pairs are a prolific source of vector mesons, which demonstrate many quantum effects. The two ions are a two-source interferometer, demonstrating interference between meson waves. Multiple vector meson production will demonstrate superradiance, a first step toward a vector meson laser. Finally, I will discuss the experimental program planned at the RHIC and LHC heavy ion colliders.

Invited talk, presented at the  
18th Advanced ICFA Beam Dynamics Workshop  
on Quantum Aspects of Beam Physics,  
October 15-20, 2000, Capri, Italy

### 1 Introduction

Heavy ion collisions might seem like a strange topic for an accelerator physics conference. However, many topics of interest to accelerator physicists also occur in peripheral heavy ion collisions. In these collisions, the ions do not physically collide. Instead, they interact electromagnetically at long ranges, up to hundreds of fermi. Relativistic heavy ions carry extremely strong electromagnetic fields, allowing tests of nonperturbative electrodynamics. These fields are strong enough to allow for multiple reactions involving a single pair of ions, so quantum fluctuations and superluminescent emission can be studied. Even for single particle production, quantum interference affects the vector meson spectrum. All of these topics have parallels in advanced accelerator design. And, some aspects of heavy ion interactions impact directly on accelerator design. This writeup will review the physics of peripheral heavy ion collisions, with an emphasis on principles. Mathematical and experimental details are left to the references.

Several different types of peripheral reactions are possible. The two nuclei may exchange one or more photons (Fig 1a). One or both nuclei may be excited

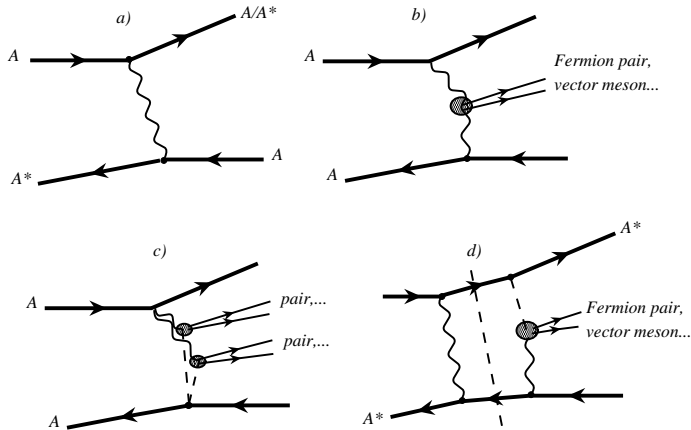


Figure 1: Some peripheral reactions: (a) Mutual nuclear excitation. (b) Two-photon interaction (c) Multiple (double) interaction, possible because  $Z\alpha$  is large. (d) Two-photon interaction with nuclear excitation. The dashed line shows how the reaction factorizes into independent two-photon (or photon-Pomeron) and nuclear excitation reactions. This is the dominant diagram; the amplitude for excitation by the photon in (b) is small<sup>7</sup>.

into a Giant Dipole Resonance (GDR) or higher state. Or, the photon may interact with a single nucleon in the nucleus in an incoherent photonuclear interaction.

Two fields may interact with each other. In a two-photon interaction, each nucleus emits a photon. The two photons collide to produce a leptonic or hadronic final state, as in Fig. 1b. The fields are so strong that ‘two-photon’ is a misnomer- the number of photons from one nucleus may be large, and, in fact, poorly defined. A photon from one nucleus may interact with the coherent meson or Pomeron fields of the other. Although this reaction has some similarities with incoherent photonuclear interactions, coherence restricts the final state kinematics, so reactions involving two coherent fields produce kinematically similar final states.

Here, we (by definition) require that the two nuclei physically miss each other and do not interact hadronically. The impact parameter  $b > 2R_A$ ,  $R_A$  being the nuclear radius. More detailed calculation will calculate and use the non-interaction probability as a function of  $b$ .

In the nuclear rest frame, a photon, Pomeron or meson coupling coherently to a nucleus must have  $p < \hbar c/R_A$ . More precisely, the coupling is governed

by the nuclear form factor. In a collider where each nucleus is Lorentz boosted by  $\gamma$ , this coupling transforms to  $p_{\perp} < \hbar c/R_A$  and photon energy  $k = p_{\parallel} < \gamma\hbar c/R_A$ . So, two-field interactions can occur up to a maximum energy  $W = 2\gamma\hbar c/R_A$ , with a final state  $p_{\perp} < 2\hbar c/R_A$ . For photons,  $p_{\perp}$  is actually smaller, peaked at  $p_{\perp} < \hbar c/b$ .

Two-photon, photon-Pomeron/meson and double-Pomeron/meson reactions are all possible. Double-Pomeron/meson interactions are limited to a narrow range of impact parameter because of the short range of the strong force. Therefore, they will occur with a relatively low cross section. They will also have a quite different  $p_{\perp}$  spectrum. The  $p_{\perp}$  spectral difference will allow some statistical separation between two-photon and photon-Pomeron interactions.

For most applications, the electromagnetic fields of ultra-relativistic nuclei may be treated as a field of virtual photons, following Weizsäcker-Williams. The photon flux from a nucleus with charge  $Z$  a distance  $r$  from a nucleus is

$$\frac{d^3 N(k, r)}{dkd^2r} = \frac{Z^2 \alpha x^2}{\pi^2 k r^2} K_1^2(x) \quad (1)$$

where  $x = kr/\gamma\hbar$  and  $K_1(x)$  is a modified Bessel function. The two-photon luminosity is the overlap of the two photon fields. The usable two-photon luminosity  $L_{\gamma\gamma}$  is this overlap, integrated over all  $b > 2R_A$ . This can be calculated using

$$L_{\gamma\gamma}(W, Y) = L_{AA} \int \frac{dk_1}{k_1} \int \frac{dk_2}{k_2} 2\pi \int_{R_A}^{\infty} b_1 db_1 \int_{R_A}^{\infty} b_2 db_2 \int_0^{2\pi} d\phi \frac{d^3 N(k_1, b_1)}{dk_1 d^2 b_1} \frac{d^3 N(k_2, b_2)}{dk_2 d^2 b_2} \Theta(b - R_1 - R_2) \quad (2)$$

where  $L_{AA}$  is the nuclear luminosity,  $\Theta$  is the step function and the impact parameter  $b = \sqrt{(b_1^2 + b_2^2 - 2b_1 b_2 \cos(\phi))}^{1/2}$ . This must be evaluated numerically. The requirement that the nuclei not physically collide ( $\Theta$  function) reduces the flux by about 50%. The final state energy  $W = 4k_1 k_2$  and rapidity  $y = 1/2 \ln(k_1/k_2)$  can also be found. Usually, the slight photon virtuality  $q^2 < (\hbar/R_A)^2$  can be neglected. The exception is  $e^+e^-$  production, since  $q^2 \sim (\hbar/R_A)^2 \gg m_e^2$ .

Since Pomerons and mesons are short-ranged, photon-Pomeron and photon/meson interactions take place inside one of the nuclei. At a given  $b$ , the photon intensity is found by integrating the photon flux over the surface of the target nucleus, and normalizing by dividing by the area  $\pi R_A^2$ . The total effective photon flux is this intensity, integrated over all  $b > 2R$ . It is found analytically; the result is within 15% of the integrated flux in the region

Table 1: Beam Species, Energies, Luminosities, compared for RHIC (Summer, 2000), RHIC Design and LHC. RHIC is expected to reach it's design parameters in 2001.

Machine	Species	Beam Energy (per nucleon)	Max. Luminosity ( $\text{cm}^{-2}\text{s}^{-1}$ )
RHIC 2000	Gold	65 GeV	$2 \times 10^{25}$
RHIC	Gold	100 GeV	$2 \times 10^{26}$
RHIC	Silicon	125 GeV	$4.4 \times 10^{28}$
LHC	Lead	2.76 TeV	$1 \times 10^{26}$
LHC	Calcium	3.5 TeV	$2 \times 10^{30}$

$b > 2R_A$ :

$$\frac{dN_\gamma}{dk} = \frac{2Z^2\alpha}{\pi k} (XK_0(X)K_1(X) - \frac{X^2}{2}[K_1^2(X) - K_0^2(X)]) \quad (3)$$

where  $X = 2R_A k/\gamma$ . For  $X < 1$ , the total number of photons with  $k_{min} < k < k_{max}$  is

$$N_\gamma = \frac{2Z^2\alpha}{\pi} \ln\left(\frac{k_{max}}{k_{min}}\right). \quad (4)$$

For photo-nuclear interactions, the maximum photon energy seen by one nucleus is strongly boosted, by  $\Gamma = 2\gamma^2 - 1$ , or 20,000 for RHIC and  $1.5 \times 10^7$  for LHC. Thus, the photon energies reach 600 GeV with gold at RHIC, and 500 TeV for lead at the LHC; with lighter nuclei, these numbers are 2-3 times higher.

Fixed target heavy ion accelerators can produce  $e^+e^-$  pairs, with and without capture; heavier states are not energetically accessible. These reactions have been studied at the LBL Bevalac, BNL AGS and CERN SPS. Studies of hadroproduction is just beginning at the Relativistic Heavy Ion Collider (RHIC) at Brookhaven National Laboratory, and the Large Hadron Collider at CERN; these colliders are energetic enough to produce a variety of final states. The characteristics of these colliders are shown in Table 1.

Peripheral collisions have recently been reviewed by Baur, Hencken and Trautmann<sup>3</sup>.

## 2 Nuclear Excitation and Incoherent Photonuclear Interactions

For low energy photons, nuclear excitations are typically collective. For example, in a Giant Dipole Resonance, the protons oscillate in one direction and the neutrons in the other. This vector oscillation can be induced by a single photon. Higher excitations include double (or higher) Giant Dipole Resonances,

Table 2: Cross sections for nuclear excitation<sup>5</sup>, pair production (Eq. 5), bound-free pair production<sup>5</sup>,  $\rho$ ,  $J/\psi$  and double- $\rho$  production<sup>16</sup>. The nuclear excitation and bound  $e^-$  cross sections are per ion.

System	$\sigma(Exc.)$	$\sigma(e^+e^-)$	$\sigma(\text{bound } e^-)$	$\sigma(\rho)$	$\sigma(J/\psi)$	$\sigma(\rho\rho)$
RHIC-Au	58 b	33 kb	45 b	590 mb	290 $\mu\text{b}$	720 $\mu\text{b}$
RHIC-Si	150 mb	41 b	1.8 mb	8.4 mb	3.6 $\mu\text{b}$	
LHC-Pb	113 b	150 kb	102 b	5.2 b	32 mb	8.8 mb
LHC-Ca	800 mb	600 b	36 mb	120 mb	390 $\mu\text{b}$	

higher  $n$  states of a harmonic oscillator. There are also Giant Quadrupole Resonances, which require multiple photons to produce. These states typically decay by emitting one or more neutrons which can be detected in far-forward calorimeters.

These reactions are of interest for a couple of reasons. As Table 2 shows, the cross sections are substantial<sup>4</sup>. Nuclear excitation is a substantial contributor to beam loss. The photon carries little momentum, so nuclear excitation creates a beam of particles with unchanged momentum but altered charge to mass ratio<sup>5</sup>. This beam will escape the magnetic optics and strike the beampipe at a relatively well defined point downstream, locally heating the magnets. This heating could cause superconducting magnets to quench. Also, this beam could be extracted from the accelerator, for fixed target use.

A single photon can excite both the emitting and target nuclei, although the cross section is smaller than for single excitation. This double process is significant for a couple of reasons. It has a clean signature and is useful as a luminosity monitor<sup>6</sup>. Second, it can tag small  $b$  events. To a good approximation, the nuclear excitation photon factorizes from the remainder of the interaction<sup>7</sup>, as is shown in Fig. 1(d). Thus the nuclear excitation can tag collisions at low  $b$ .

### 3 Two-Photon Interactions

Two-photon interactions have been studied extensively at  $e^+e^-$  colliders. Photons couple to charge, so two-photon couplings measure the internal charge content of mesons;  $q\bar{q}$  pairs are produced, but not charge-free states like glueballs. Hybrids ( $q\bar{q}g$ ) and 4-quark states ( $q\bar{q}q\bar{q}$ ) are produced at intermediate rates. Thus, coupling to two-photons is a sensitive test for exotic mesons.

Meson pair production rates depend on the pair energy. Near threshold, charged meson pairs ( $\pi^+\pi^-$ ) are produced, but neutral pairs ( $\pi^0\pi^0$ ) are not. At higher energies, the photons see the quark structure of mesons, and both

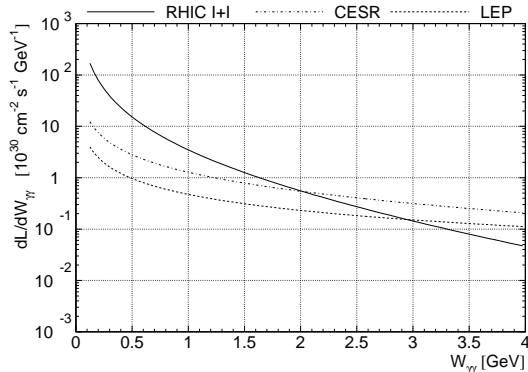


Figure 2: Two-photon luminosity expected at RHIC with gold and iodine beams, compared with the luminosities at LEP II ( $\sqrt{s} = 180$  GeV and a luminosity of  $5 \times 10^{31} \text{cm}^{-2} \text{s}^{-1}$ ) and at CESR ( $\sqrt{s} = 10$  GeV and a luminosity of  $2.9 \times 10^{32} \text{cm}^{-2} \text{s}^{-1}$ ).

charged and neutral mesons are produced.

Two-photon interactions at heavy ion colliders are of interest because that the luminosity scales as  $Z^4$  and extremely high rates are possible. Figure 2 compares the  $\gamma\gamma$  luminosities at RHIC, with the LEP and CESR  $e^+e^-$  colliders<sup>8</sup>; for  $W < 1.5$  GeV, RHIC can reach the highest presently available two-photon luminosities. Heavy ion colliders also probe some unique areas, such as multiple pair production, and bound-free pair production; both are probes of strong field QED.

### 3.1 Lepton Pair Production

Lepton pair production can test the limits of perturbative QED. Perturbation theory may fail because the coupling  $A\alpha$  is so large. Even with perturbative approaches,  $e^+e^-$  production introduces additional complications. The electron Compton wavelength,  $\Lambda_e = 386$  fm, is large compared to typical impact parameters. So at  $W \sim 2m_e$ , where the bulk of the cross section is, the pair production is poorly localized.

The first perturbative calculation specific to heavy ion collisions was by Bottcher and Strayer<sup>9</sup>. They treated the ions as sources of classical (but relativistic) electromagnetic potentials that follow fixed trajectories. This approach naturally incorporated off-shell photons. This calculation also accounted for large electron Compton radius  $\Lambda_e = 386$  fermi, with an appropriate cutoff. In the two-photon approach,  $\Lambda_e$  should replace the minimum impact

parameter,  $R_A \sim 7$  fermi, in Eq. 2. This reduces the cross section significantly compared to earlier calculations.

A slightly later, more refined calculation by Baur and Bertulani included Coulomb corrections, to account for the fact that the pair is produced deep in a Coulomb potential<sup>10</sup>. With this refinement, the cross section is given by

$$\sigma = \frac{28Z^4\alpha^4\hbar^2}{27\pi m_e^2 c^2} \left( \ln^3\left(\frac{\Gamma\delta}{2}\right) - \frac{3}{2}(1 + 2\bar{f}) \ln^2\left(\frac{\Gamma\delta}{2}\right) \right) \quad (5)$$

where  $m_e$  is the electron mass,  $\delta = 0.681$  is Euler's constant and  $\bar{f} = (Z\alpha)^2 \Sigma_{n=1}^{\infty} [n(n^2 + Z^2\alpha^2)]^{-1}$  is the usual Coulomb correction. The  $\ln^3$  term dominates at high energy. Other authors have found slightly different results, depending on the details of the calculation.

Baur and Bertulani also calculated the probability of pair production at a given  $b$ . With gold at RHIC, this probability is greater than 1 for  $b = \Lambda_e$ ! The differential cross section  $d\sigma/2\pi b db$  saturates. The problem is resolved by multiple pair production: a single ion pair small- $b$  confrontation can produce more than one pair. The the number of pairs is Poisson distributed, with the  $b$ -dependent mean<sup>11</sup>. This saturation can also affect calculations of the single pair cross section.

Numerous authors have considered non-perturbative  $e^+e^-$  production, usually using the time-dependent Dirac equation. Some authors solved the coupled-channel equations numerically. The ions were stepped through their positions. At each step, the coupling from the initial state to a pair-containing final states was calculated. An accurate calculation requires a complete and orthogonal set of states. This turned out to be rather difficult, and early calculations found results that varied by orders of magnitude.

Baltz and McLerran calculated pair production to all orders<sup>12</sup>. Their method is similar to the perturbative calculation. They worked in light-cone coordinates with Lienard-Wiechert potentials similar to those of Bottcher & Streyer. They first found the Greens function for the exact wave function at the interaction point. The transition amplitude was then constructed from the Greens function. The total cross section is this amplitude, integrated over impact parameter and intermediate transverse momentum. Their result matches the perturbative result (without Coulomb corrections).

Recently, Roman Lee and A. Milstein found a problem with the order of integration in the Baltz and McLerran paper<sup>13</sup>. When the order changed, Lee and Milstein the result changed to include the Coulomb correction found by Baur & Bertulani (the  $\bar{f}$  term in Eq. 5).

The agreement with perturbation theory is somewhat surprising, given the large coupling. However, Baltz and McLerran found that, for multiple

pair production, their result was smaller than the perturbative result. Since multiple pair production is naturally a higher order process, it's not surprising that a difference appears.

A related reaction is bound-free pair production where the electron is produced bound to one of the nuclei. As with free pairs, perturbative calculations may be inadequate, and an exact solution to the time-dependent Dirac equation is desired. This problem has also been tackled perturbatively; here the final state consists of a free positron and an electron in an atomic orbital. The cross section to produce an electron bound in an atomic  $K$ -shell is<sup>3</sup>

$$\sigma = \frac{33\pi Z^8 \alpha^8 \hbar^2}{10m_e^2 c^2} \frac{1}{\exp(2\pi Z\alpha) - 1} \left[ \ln\left(\frac{\Gamma\delta}{2}\right) - \frac{5}{3} \right]. \quad (6)$$

The stronger  $Z$  dependence comes from the electron-nucleus binding energy. Inclusion of higher shells will increase this by about 20%. This cross section has the form  $\sigma = A \ln(\gamma) + B$ . Extrapolations from lower energy data using this form find a cross section about twice as large<sup>14</sup>. Coupled-channel calculations have been tried on this problem, and produced a wide range of results. Also, as with free-production, an all-order solution to the time-dependent Dirac equation has recently been found, again using light-cone coordinates<sup>15</sup>. The result was slightly lower than perturbation theory. The cross section for bound-free production is much lower than for free production, so that  $d\sigma/2\pi b db$  is not saturated.

The 1-electron atoms produced in this reaction have their momentum unchanged, so that they will follow well-defined trajectories. As with nuclear excitation, this can lead to heating of the accelerator magnets and also allow for extracted beams<sup>5</sup>.

In principle, these non-perturbative aspects of pair production also apply to  $\mu^+\mu^-$  and  $\tau^+\tau^-$  production. However, the masses are much larger, so any non-perturbative effects are much smaller. Because  $m_\mu > \hbar/R_A$ , Eq. 2 applies for heavy lepton production.

#### 4 $q\bar{q}$ fluctuations and Vector Meson Production

The vacuum fluctuation  $\gamma \rightarrow q\bar{q}$  is similar to  $\gamma \rightarrow e^+e^-$ ; only the final state charges and masses are different. Just as the virtual  $e^+e^-$  pair can interact with an external Coulomb field and become real, the  $q\bar{q}$  pair can interact with an external nuclear field and emerge as real vector meson<sup>16</sup>.

This picture is clearest in the target rest frame. The incoming photon has a high momentum, and the fluctuation persists for a time  $\tau_f = \hbar/M$ , during which it travels a distance known as the formation distance  $l_f = 2\hbar k/M^2$ . In



alternate language,  $l_f = \hbar/p_{||}$ , where  $p_{||}$  is the momentum transfer required to make the pair real. For  $e^+e^-$  pairs,  $l_f$  is typically much larger than a single atom; for  $q\bar{q}$  pairs,  $l_f$  is typically much larger than a single nucleus. So, the fluctuation cannot see the target structure. During its lifetime, the fluctuation can interact with the external field to become a real pair.

The  $q\bar{q}$  scatters elastically from the a nucleus with atomic number  $A$ . This scattering is mediated by the strong force and transfers enough momentum to give the meson its mass. The scattering leaves the photon quantum numbers  $J^{PC}$  unchanged. This elastic scattering cannot easily be described in terms of quarks and gluons. The most successful description is in terms of the Pomeron<sup>17</sup>. For hard processes the Pomeron may be thought of as a 2-gluon (quasi-bound) ladder, connected by gluon rungs. However, for soft processes such as elastic scattering, this picture may be inappropriate. For soft reactions, the best picture is the 40-year old soft-Pomeron diffractive picture<sup>18</sup>. The Pomeron absorbs part of the photon wave function, allowing a  $q\bar{q}$  to emerge dominant.

In this model, the cross section for the reaction  $A + A \rightarrow A + A + V$  may be calculated in a straightforward manner. The starting point is data on  $\gamma + p \rightarrow V + p$  from fixed target experiments and HERA. The forward scattering amplitudes may be parameterized  $d\sigma/dt|_{t=0} = b_v(XW^\epsilon + YW^{-\eta})$ , where  $t$  is the 4-momentum transfer from the nucleus and here  $W$  is the  $\gamma p$  center of mass energy. The first term, with  $\epsilon \sim 0.22$ , is for Pomeron exchange, while the second is for meson exchange; Pomeron exchange dominates at high energies. This amplitude factorizes into two parts: the  $\gamma \rightarrow q\bar{q}$  amplitude and the elastic scattering amplitude. The first part can be determined from the partial width for  $V \rightarrow e^+e^-$ , allowing vector meson production data to fix the scattering amplitude. Vector meson dominance allows us to treat the  $q\bar{q}$  fluctuation as a real vector meson. The optical theorem can be used to find the total  $Vp$  cross section.

The total  $VA$  cross section may be found with a Glauber calculation. This calculation integrates over the transverse plane, summing the probability of having 1 or more interactions:

$$\sigma_{tot}(VA) = \int d^2\vec{r}(1 - e^{-\sigma_{tot}(Vp)T_{AA}(\vec{r})}) \quad (7)$$

where  $T_{AA}(\vec{r})$  is the nuclear thickness function. These cross sections rise with  $W$  at low energies, then level off at an almost constant value.

The optical theorem is used to find  $d\sigma/dt|_{t=0}$  for the meson -nucleus scattering. Finally, the leptonic width is used to find the forward amplitude for vector meson production. In the small- $\sigma$  limit,  $\sigma_{tot}(Vp)T_{AA}(b=0) \ll 1$ , the

forward amplitude scales as  $A^2$ . This limit applies for heavy systems such as  $c\bar{c}$ . As  $\sigma_{tot}(Vp)$  rises, the  $A$ -dependence decreases, and for large  $\sigma_{tot}(Vp)$ , the scaling is  $A^{4/3}$ , with the vector meson seeing the front face of the nucleus.

The total photonuclear cross section is given by an integration over  $t$ :

$$\sigma(\gamma A \rightarrow VA) = d\sigma/dt(\gamma A \rightarrow VA)|_{t=0} \int_{t_{min}}^{\infty} dt |F(t)|^2 \quad (8)$$

where  $t_{min} = M_V^2/4k$  and  $F(t)$  is the nuclear form factor. For a heavy nucleus,  $F(t)$  may be fit analytically by a convolution of a hard sphere with a Yukawa potential.

Eq. 8 agrees well with data from fixed target experiments. The total cross section is

$$\sigma(A + A \rightarrow A + A + V) = 2 \int dk \frac{dN_\gamma}{dk} \sigma(\gamma A \rightarrow VA). \quad (9)$$

The factor of 2 is because either nuclei can act as target or emitter. These cross sections are given in Table 2.

The implications of this straightforward calculation are significant. The cross sections are huge. With gold at RHIC,  $\rho^0$  production is 10% of the total hadronic cross section. With lead at LHC, the  $\rho^0$  cross section is about equal to the hadronic cross section! Heavy ion colliders can act as vector meson factories, with rates comparable to  $e^+e^-$  vector meson machines. The  $10^{10}$   $\phi$  produced in  $10^6$  seconds with calcium beams at LHC is comparable to that expected at a dedicated  $\phi$  factory. Searches for rare decay modes, CP violation and the like are possible. Also, vector meson spectroscopy will be productive; mesons like the  $\rho(1450)$ ,  $\rho(1700)$  and  $\phi(1680)$  will be copiously produced.

Fully coherent final states will be distinctive. The final state  $p_\perp$  is a convolution of the photon and Pomeron  $p_\perp$ . Figure 3 shows these contributions. The mean  $p_\perp$  from the photon is  $\hbar/b$ , considerably smaller than  $\hbar/R_A$ .

This approach can also find the vector meson rapidity distribution. The final state rapidity  $y = 1/2 \ln(M_V/k)$ . So,  $d\sigma/dy = k/2 d\sigma/dk$  and can be determined from Eq. 9. The photon can come from either direction, so the total  $\sigma(y)$  includes contributions for photons from  $+y$  and  $-y$ .  $d\sigma/dy$  is shown in Fig. 4.

#### 4.1 Interference

The observed  $p_\perp$  spectrum is more complicated than Fig. 3 shows. Either nucleus can emit the photon. The two possibilities are indistinguishable, and

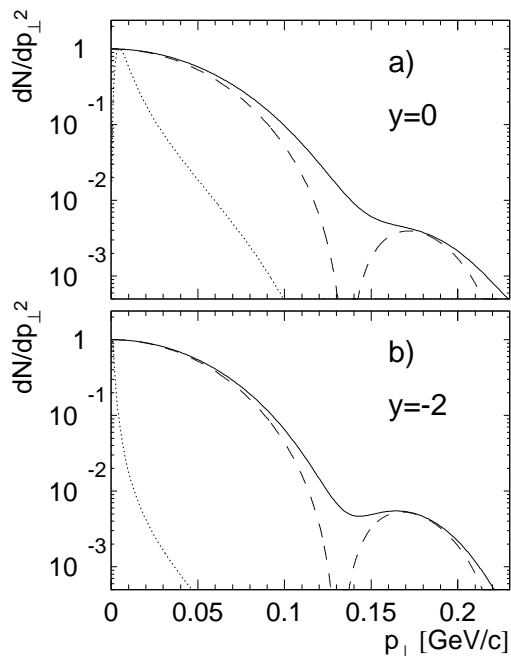


Figure 3: The vector meson  $p_{\perp}$  spectrum (solid line) at  $y = 0$  (a) and  $y = 2$  (b) is the convolution of the photon  $p_{\perp}$  (dotted line) and the scattering  $p_{\perp}$  transfer (dashed line).

therefore, they interfere. In essence, the two nuclei act as a two-source interferometer. The two possible emitters are related by a parity transformation. Vector mesons are negative parity so the two possibilities contribute with opposite signs, producing destructive interference<sup>19</sup>. The cross section is

$$\sigma(p_{\perp}, y, b) = A^2(p_{\perp}, y, b) + A^2(p_{\perp}, -y, b) - 2A(p_{\perp}, y, b)A(p_{\perp}, -y, b) \cos(\phi(y) - \phi(-y) + \vec{p}_{\perp} \cdot \vec{b}) \quad (10)$$

where  $A(p_{\perp}, -y, b)$  is the production amplitude and  $\phi(y)$  is the production phase.  $A$  may be found from the previous section. For pure Pomeron exchange, the production is almost real. The production phase always cancels at  $y = 0$ , and cancels everywhere unless  $\phi$  depends on  $k$ . Variation is likely with the  $\rho$  and  $\omega$  because of the meson contribution. For other mesons, it is likely to be small or negligible.

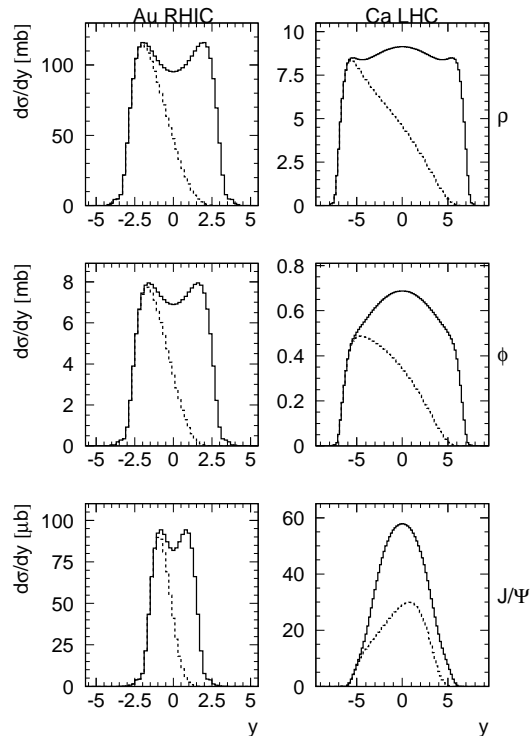


Figure 4: Rapidity distribution  $d\sigma/dy$  with gold at RHIC (left panels) and calcium at the LHC (right panels) for the  $\rho^0$ ,  $\phi$  and  $J/\psi$ . The solid line is the total, while the dashed line shows the production for a single photon direction.

At midrapidity, the interference simplifies to

$$\sigma(p_{\perp}, y = 0, b) = A^2(p_{\perp}, y = 0, b)(1 - \cos[\vec{p} \cdot \vec{b}]). \quad (11)$$

For a given  $b$ ,  $\sigma$  oscillates with period  $\Delta p_{\perp} = \hbar/b$ . When  $p_{\perp}b < \hbar$ , the interference is destructive and there is little emission. The mean  $b$  for  $\rho$  production at RHIC is about 40 fermi, rising to 300 fermi at LHC.

The impact parameter is unmeasured, so it is necessary to integrate over all  $b$ . This dilutes the interference, except for  $p_{\perp} < \hbar/\langle b \rangle$ . Figure 5 shows the expected  $p_{\perp}$  spectrum with and without interference.

The mean impact parameter for  $\rho$  production with gold at RHIC is 40 fermi, far larger than the rho decay distance  $\gamma\beta c\tau < 1$  fermi. The vector

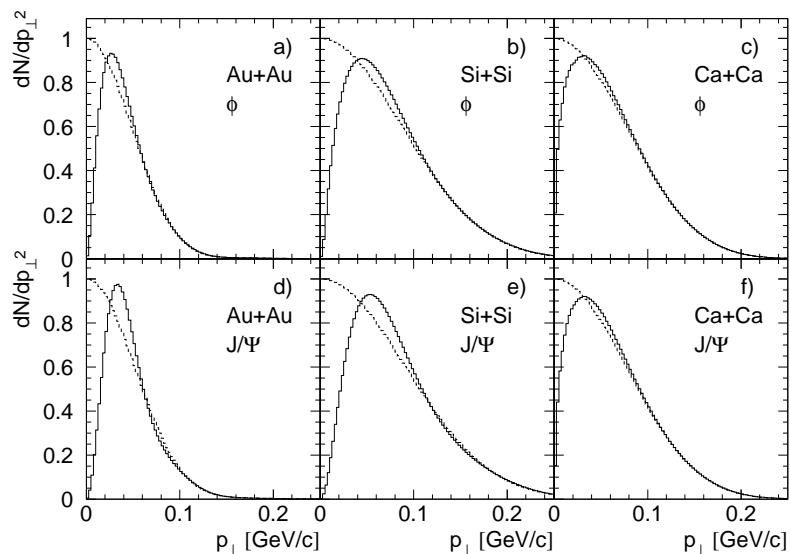


Figure 5: Meson  $p_{\perp}$  spectra, with (solid lines) and without (dashed line) interference, at  $y=0$ . The top panels are for the  $\phi$ , and the bottom for the  $J/\psi$ , with gold (left) and silicon (center) at RHIC, and calcium at the LHC (right).

mesons decay before their wave functions can overlap! However, the decay product do overlap and interfere. The angular distributions for the two  $\rho^0$  sources are the same, so the interference pattern is not affected. This process requires a non-local wave function. Consider  $\rho^0 \rightarrow \pi^+\pi^-$ , with  $b \sim 40$  fermi. Before the  $\pi^+$  waves from the 2 sources can overlap, they must travel  $\sim 20$  fermi each, during which time the  $\pi^-$  waves will travel 20 fermi in the opposite direction, and the  $\pi^+$  and  $\pi^-$  waves will be separated by 40 fermi. So, non-locality is required to produce this interference pattern.

Although there is as yet no counterpart to Bell's inequality, the choice of quantum observable does matter for this system. Consider a system where  $b$  is measured. For the  $\pi^+$  and  $\pi^-$ , one can measure either the momentum or position. If the momenta of both  $\pi$  are measured, then the interference pattern is observed. If the  $\pi^+$  momentum is known, that disallows certain values of  $\pi^-$  momentum where destructive interference is complete. If the positions of both  $\pi$  are measured, the production point can be determined, but the interference disappears. If one position and one momentum are observed, neither the interference pattern nor the production point can be determined.

The wave function of the system is

$$\Psi(\vec{x}) = \exp(i(\vec{k}_- + \vec{k}_+) \cdot \vec{x}) [\exp(i(\vec{k}_- + \vec{k}_+) \cdot \vec{R}_A) - \exp(i(\vec{k}_- + \vec{k}_+) \cdot \vec{R}_B)] \quad (12)$$

where  $\vec{x}$  is where the vector meson would be if it didn't decay; in the vector meson rest frame  $\vec{x} = 1/2(\vec{x}_+ + \vec{x}_-)$  where  $\vec{x}_+$  and  $\vec{x}_-$  are the position for the  $\pi^+$  and  $\pi^-$ , and  $\vec{k}_+$  and  $\vec{k}_-$  their momenta. This wave function cannot be factorized:  $\Psi(\pi^+\pi^-) \neq \Psi(\pi^+)\Psi(\pi^-)$ . Since the  $\pi^+$  and  $\pi^-$  are well separated, the wave function is non-local. This system is thus an example of the Einstein-Podolsky-Rosen paradox.

#### 4.2 Multiple Vector Meson Production

The vector meson production probability at a given  $b$  may be calculated with the impact-parameter dependent photon flux. This is shown in Fig. 6. At  $b = 2R$ , the probability of  $\rho^0$  production is 1% at RHIC, rising to 3% at LHC. These probabilities are high enough that multiple meson production should be observable. In the absence of quantum or other correlations, multiple meson production should be independent and Poisson distributed. At  $b = 2R$ , the  $\rho^0\rho^0$  probabilities are  $(1\%)^2/2$  and  $(3\%)^2/2$  at RHIC and LHC respectively. After integration over  $b$ , 1.4 million  $\rho^0\rho^0$  are expected per year at RHIC. Like meson triples should also be produced in observable numbers. Vector mesons are bosons so production of like-meson pairs should be enhanced for momentum differences  $\delta p < \hbar/R_A$ . The meson follows the photon spin and can be aligned or anti-aligned with the beam direction, so the enhancement is only 50%, so  $N(\text{pair}) \sim 1 + 0.5 \exp(\delta p R_A / \hbar)$ .

## 5 Experimental Status

Fixed target measurements have been published for pair production, with and without capture, and nuclear excitation. Due to space limitations, this writeup will only consider relativistic collisions, with  $\Gamma > 10$ . The solid targets, with the nuclei surrounded by their electron clouds, differ from the stripped ion collisions we focus on here. Measurements of pair production in sulfur on heavy ion collisions around  $\Gamma = 160$  have matched theoretical predictions<sup>20</sup>. Pair production with capture has also been studied with lead beams<sup>14</sup>. As was previously mentioned, when scaled to RHIC and LHC energies, this data may exceed current estimates. However, corrections may be needed for the limited boost of the current experiments.

Programs to study a variety of peripheral reactions are underway in the STAR collaboration at RHIC and the CMS collaboration at LHC. For most

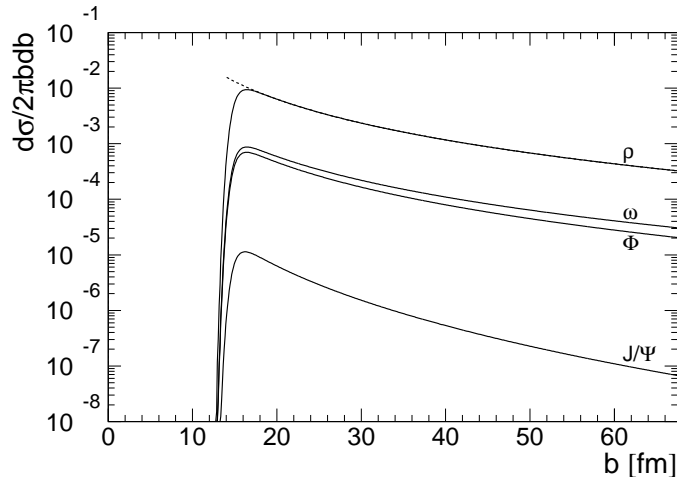


Figure 6: Probability of meson production, with gold at RHIC, as a function of  $b$ .

reactions, the largest backgrounds are expected to be grazing hadronic collisions, beam gas interactions, and incoherent photonuclear interactions<sup>8</sup>. For triggering, debris from upstream interactions, and cosmic ray muons can be important.

These backgrounds can be separated from the signals by selecting events with low multiplicity, typically, 2 or 4, low total  $p_{\perp}$ , and zero net charge. Baryon number and strangeness must also be conserved.

At the trigger level, significant rejection can be achieved by requiring that the event originate inside the interaction region; this removes most of the beam gas events, along with almost all of the upstream interactions and cosmic ray muons. Event timing cuts also help reject cosmic ray muons.

The STAR detector combines a large acceptance with a flexible trigger<sup>21</sup>. Charged particles are detected in the pseudorapidity range  $|\eta| < 2$  and  $2.4 < |\eta| < 4$  by a large central time projection chamber (TPC) and two forward TPCs. This TPC can also identify particles by  $dE/dx$ . Neutral particles are detected by a central barrel ( $|\eta| < 1$ ) and endcap ( $1 < \eta < 2$ ) calorimeter. Two zero degree calorimeters will detect neutrons from nuclear breakup, useful for background rejection.

For triggering, a scintillator barrel covering  $|\eta| < 1$  and multi-wire proportional chambers covering  $1 < |\eta| < 2$  measure charged particle multiplicity on an event by event basis. These detectors have good segmentation, allowing

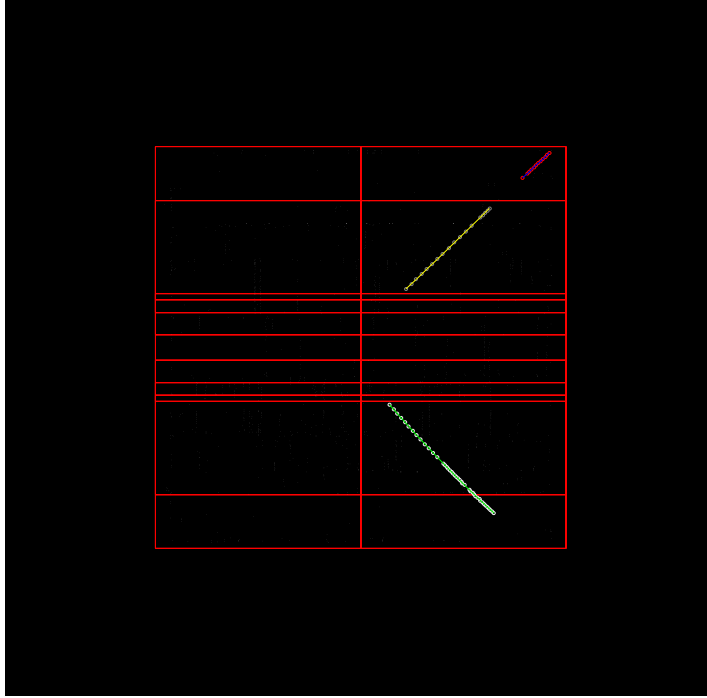


Figure 7: Side view of an event collected with the peripheral collisions trigger. The invariant mass and  $p_{\perp}$  are consistent with coherent  $\rho^0$  production.

for total multiplicity and topological selection in the trigger. The trigger has 4 levels, with the earliest level based on field programmable gate arrays and the later levels computer based. The final selection uses on-line TPC tracking. Peripheral collisions data will be collected in parallel with central collision data. Simulations show that the planned trigger algorithms should be able to efficiently select peripheral events while rejecting enough background enough to minimize downtime<sup>8</sup>.

STAR took its first data this summer (2000). The central TPC, scintillator barrel and zero degree calorimeters were operational. Although the trigger was not completely functional, in late August, the collaboration took about 7 hours of data with a dedicated trigger optimized to select 2-track peripheral events<sup>22</sup>. The trigger rate of 20-40 Hz was filtered to 1-2 Hz by the final trigger, which reconstructed the tracks on-line. About 20,000 events were written to tape.

The initial event selection required a 2-oppositely-charged track, primary vertex in the interaction diamond. The tracks were required to be at least slightly acoplanar to eliminate cosmic ray muons, and the event had to have a small  $p_{\perp}$ . About 300 events passed these cuts. This data is now being analyzed for signals from  $e^+e^-$  pair and  $\rho^0$  production - the two processes



with the largest cross sections. Figure 7 shows an example of a  $\rho^0$  candidate.

The CMS collaboration plans to study peripheral collisions with lead and calcium beams at LHC<sup>23</sup>. Their plans are at a fairly early stage.

## 6 Conclusions

Peripheral collisions of heavy nuclei can probe a wide variety of phenomena, including many faces of strong QED. Production of  $e^+e^-$  and  $q\bar{q}$  pairs can probe the electrodynamics of the vacuum. Besides the physics interest, peripheral collisions affect many other areas, as a tool for hadron spectroscopy, and impacting accelerator design,

After many years of theoretical discussion, experimental results are beginning to become available.

## Acknowledgements

I would like to acknowledge Joakim Nystrand, my collaborator in the studies of vector mesons. This work was supported by the U.S. DOE, under Contract No. DE-Ac-03-76SF00098.

## References

1. G. Baur and L.G. Ferreira Filho, Nucl. Phys. **A518**, 786 (1990).
2. R. N. Cahn and J. D. Jackson, Phys. Rev. **D42**, 3690 (1990).
3. G. Baur, K. Hencken and D. Trautmann, J. Phys. G **24**, 1657 (1998).
4. M. Vidovic, M. Greiner and G. Soff, Phys. Rev. **C48**, 2011 (1993).
5. S. Klein, physics/005032, to appear in Nucl. Instrum. Meth.
6. A. J. Baltz, C. Chasman and S. N. White, Nucl. Instrum. Meth **A417**, 1 (1998).
7. K. Hencken, D. Trautmann and G. Baur, Z. Phys. **C68**, 473 (1995).
8. J. Nystrand and S. Klein, in *Proc. Wkshp. on Photon Interactions and Photon Structure*, Lund, Sweden, 1998 ed. G. Jarlskog and T. Sjöstrand; nucl-ex/9811007.
9. C. Bottcher and M. R. Strayer, Phys. Rev. **D39**, 1330 (1989).
10. C. A. Bertulani and G. Baur, Phys. Rep. **163**, 299 (1998).
11. K. Hencken, D. Trautmann and G. Baur, Phys. Rev. **C59**, 841 (1999).
12. A. J. Baltz and Larry McLerran, Phys. Rev. **C58**, 1679 (1998).
13. R. Lee, contribution to this conference; R. Lee and A. I. Milstein, Phys. Rev. **A61**, 032103 (2000).
14. P. Grafström *et al.*, *Measurement of electromagnetic cross sections in heavy ion interactions and its consequence for luminosity lifetimes in ion*

- colliders*, CERN-SL-99-033 EA.
15. A. J. Baltz, Phys. Rev. Lett. **78**, 1231 (1997).
  16. S. R. Klein and J. Nystrand, Phys. Rev. **C60**, 014903 (1999).
  17. *Quantum Chromodynamics and the Pomeron*, by J. R. Forshaw and D. A. Ross, Cambridge University Press, 1997, is a good discussion of the modern Pomeron. For a more traditional approach, see Ref. 6.
  18. T. H. Bauer, R. D. Spital, D. R. Yennie and F. M. Pipkin, Rev. Mod. Phys. **50**, 261 (1978).
  19. S. R. Klein and J. Nystrand, Phys. Rev. Lett. **84**, 2330 (2000).
  20. R. Baur *et al.*, Phys. Lett. **B332**, 471 (1994); C. R. Vanes *et al.*, Phys. Rev. Lett. **69**, 1711 (1992).
  21. K. H. Ackermann *et al.*, Nucl. Phys. **A661**, 681 (1999).
  22. J. Seger, presented at the 2000 APS Division of Nuclear Physics Meeting, Oct. 4-7, 2000, Williamsburg, VA. Transparencies are available on the web at <http://www-rnc.lbl.gov/STAR/conf/talks2000/dnp/seger.pdf>.
  23. G. Baur *et al.*, hep-ph/9904361.